JOURNAL OF CATALYSIS 124, 503–510 (1990)

Decavanadate Ion-Pillared Hydrotalcite: Spectroscopic Studies of the Thermal Decomposition Process

JEN TWU AND PRABIR K. DUTTA

Department of Chemistry, The Ohio State University, 120 West 18th Avenue, Columbus, Ohio 43210

Received December 19, 1989; revised February 26, 1990.

In this study, we have focused on the thermal decomposition of the material generated by ion-exchange of decavanadate ions into the layers of a magnesium aluminum hydroxide hydrotalcite-like compound, over the temperature range from ambient to 650°C. Using powder diffraction data and Raman and XANES spectroscopy, it was found that the intercalated decavanadate ions transform into cyclic and chain-like metavanadate species at temperatures between 160–350°C. The metal hydroxide layer structure remains intact until 350°C. Reaction between the metal oxide and the metavanadate species to form magnesium vanadates is only observed for samples heated in excess of 450°C.

INTRODUCTION

Layered materials that are characterized by structures held together by strong covalent bonds in the *xy* plane but considerably weaker bonds in the *z* direction include materials such as graphite, silicic acids, zirconium phosphates, smectites and hydrotalcite minerals (*1–5*). The weakness of bonding in the *z* direction can be readily exploited to introduce atoms, molecules, and ions into the interlayer space, thereby generating a diverse group of materials with applications in technologies involving batteries, catalysts, and ionic conductors (*6–8*).

Of particular interest to this paper are the materials resembling the minerals belonging to the pyroaurite–sjogrenite type, represented by the general formula $[M^{II}_{1-x}M^{III}_x(OH)_2]\,A^{n-}_{x/n}\cdot z\,H_2O$, where M^{II} = Mg, Zn, Fe, Co, Ni, Cu and M^{III} = Al, Cr, Fe (*9*). As an example, the structure of the mineral hydrotalcite in this group $Mg_2Al(OH)_6\cdot Cl$ can be thought of as derived from brucite ($Mg(OH)_2$), in which the Mg^{+2} cations are octahedrally surrounded by edge-sharing -OH groups in a layer. The layers are stacked upon each other. Replacement of a certain fraction of the divalent cations by trivalent cations such as Al^{+3} leads to a positively charged metal hydroxide layer, necessitating the presence of anions such as Cl^- in the interlayer space (*10*). A large variety of ions can be introduced into these materials (*11–17*). These systems are therefore complementary to the more commonly occurring cationic clays, in which cations such as Na^+, K^+ in the interlayers neutralize the negatively charged aluminosilicate sheets. Considerable work has been done in order to generate novel catalytic materials by pillaring the aluminosilicate layers in smectite-type cationic clays with polyhydroxoaluminum and zirconium cations (*18–20*). The unique catalytic properties of these materials stem from the novel acidic sites, the thermal stability, and the large internal surface area.

Pinnavaia and co-workers have recently shown that it is possible to introduce polyoxometalate ions as pillars into layered metal hydroxides (*21*). The decavanadate ion ($V_{10}O_{28}^{-6}$) was exchanged into the layers of $Zn_2Al(OH)_6^+$, $Zn_2Cr(OH)_6^+$, and $Ni_3Al(OH)_8^+$. Drezdzon has also reported the exchange of $V_{10}O_{28}^{-6}$ and $Mo_7O_{24}^{-6}$ into $Mg_2Al(OH)_6^+$ via an intermediate terephthal-

0021-9517/90 $3.00

ate derivative (*22*). Complex Keggin ion structures have also been introduced into the $Zn_2Al(OH)_6^+$ material (*23*). Drezdzon, based on thermal analysis data, concluded that the heptamolybdate- and decavanadate-pillared hydrotalcites are stable above 500°C (*22*). We have recently reported on the ion-exchange of vanadates into the layered hydroxide $LiAl_2(OH)_6^+$ (*17*). Over the pH range of 3–11, the predominant species ion-exchanged into the lithium aluminate were $V_2O_7^{-4}$ and $V_4O_{12}^{-4}$. Thermal treatment of $LiAl_2(OH)_6^+$–$\frac{1}{4}$ V_2O_7 was examined and it was found that the $V_2O_7^{-4}$ dimerizes to $V_4O_{12}^{-4}$ around 100°C. The interlayer polymerization proceeds up to temperatures of 350°C, with formation of polymeric metavanadates in the interlayer. At higher temperatures, degradation of the frame work occurs, with ultimate formation of Li_3VO_4 and $LiVO_3$.

Like their counterparts of pillared smectite clays, interest in these polyoxometalate–hydrotalcite materials also stems from their potential use as catalytic materials. A patent in 1984 refers to their use for exhaust gas and hydrocarbon conversion catalysts (*24*). Thermal decomposition of various layered hydroxides have led to catalysts active for aldol condensation, olefin isomerization, β-propiolactone polymerization, and methanol synthesis via water–gas shift reaction (*25–28*). Photooxidation of isopropyl alcohol and selective oxidation of xylene to tolualdehyde have been reported for the polyvanadate–hydrotalcite systems, similar to the materials discussed in this paper (*17, 21*).

In this study, we focus on the $V_{10}O_{28}$–$Mg_2Al(OH)_6$ system, synthesized by procedures similar to that described by Drezdzon (*22*). We have followed the interlayer chemistry upon thermal decomposition of this system by X-ray diffraction, Raman spectroscopy, and X-ray absorption near-edge spectroscopy (XANES), and have correlated these data to provide a consistent model.

The relevance of the structural studies described in this paper to catalytic applications of these materials arises from several factors. It is obviously of importance to establish the exact nature of the intercalating anion and its interaction with the layered hydroxide framework, especially under conditions typical of catalytic reactions. This paper shows that Raman spectroscopy provides a powerful probe for examining the structure of the interlayer species and their reactivity upon thermal treatment.

EXPERIMENTAL

Analytical reagent grade chemicals from Aldrich were used for preparation of all the samples described in this work. Preparation of the decavanadate-pillared hydrotalcite was adapted from the procedure described by Drezdzon (*22*). To a solution of 14 g of terephthalic, 30 g of NaOH, and 200 ml of H_2O was added a solution of 40 g of $Mg(NO_3)_2 \cdot H_2O$, 30 g of $Al(NO_3)_3 \cdot 9H_2O$, and 125 ml of H_2O. This mixture was heated at 90°C for 24 h, separated by centrifugation, and thoroughly washed. The exchange of the terephthalate with vanadate was carried out with a solution of 20 g of $NaVO_3$ in 100 ml of H_2O adjusted to a pH of 4.5 with 2 *M* HNO_3. Thermal treatment of the decavanadate–hydrotalcite samples was carried out in an oven manufactured by Technical Products Corp.

Powder X-ray diffraction patterns were obtained with a Rigaku Geigerflex D/Max 2B using nickel-filtered Cu$K\alpha$ radiation. Raman spectra were recorded with excitation from a Spectra Physics Argon Ion Laser (Model 170) and the scattered light was collected and dispersed with a Spex 1403 double monochromator and detected by a C 31034 GaAs photomultiplier tube. Typical power at the sample was between 10–20 mW. The slit widths were 6 cm^{-1} and scan times of 1–3 s/cm^{-1} were used. XANES measurements in the fluorescence mode were carried out at the National Synchrotron Light Source, Brookhaven National Laboratory (beam line X-9A), with an electron energy of 2.5 GeV and ring currents

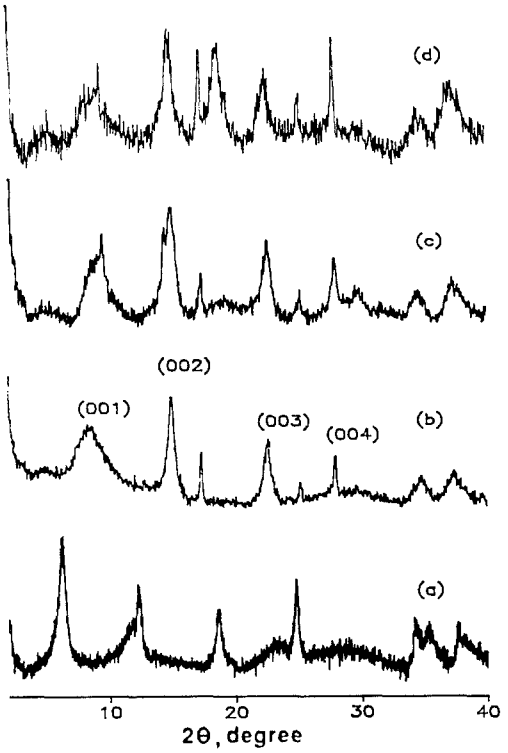

FIG. 1. Powder X-ray diffraction patterns of (a) terephthalate–$Mg_2Al(OH)_6^+$ and (b) $V_{10}O_{28}$–$Mg_2Al(OH)_6$ at room temperature and heated to (c) 100°C and (d) 160°C (12 h at each temperature).

between 100 and 200 mA. Data were collected at the V *K*-edge (5465 eV). A Si(111) crystal monochromator was used for selecting the appropriate wavelength.

RESULTS

The decavanadate ion was exchanged into the $Mg_2Al(OH)_6^+$ material by replacing the terephthalate ion using an aqueous vanadate solution at pH 4.5, as described in the literature (*22*). Figures 1a and 1b show the powder pattern for the phthalate–hydrotalcite sample and upon ion-exchange by vanadate. The (001) reflections are marked on the figure and are in agreement with previous studies (*21, 22*). The basal spacing (d_{001}) corresponding to these reflections is 11.9 Å and leads to a gallery height of 7.1 Å, indicating a $V_{10}O_{28}^{-6}$ orientation with the C_2 axis parallel to the layers (*21, 22*). The Raman spectrum of this vanadate-exchanged material is shown in Fig. 2b and is compared to $V_{10}O_{28}^{-6}$ in solution (Fig. 2a). Although the *S/N* of the spectrum for the hydrotalcite is poorer than that of the solution, it is quite clear that all the characteristic peaks of the decavanadate ion at 320, 454, 534, 595, 834, 975, and 998 cm^{-1} are clearly observed in the hydrotalcite samples (*29*). No other Raman bands characteristic of $V_2O_7^{-4}$ or $V_4O_{12}^{-4}$ are observed (*29*). Therefore, the Raman spectrum provides an unambiguous description of the intercalated species.

The powder pattern and Raman spectrum of the $V_{10}O_{28}$–$Mg_2Al(OH)_6$ sample heated to 100°C for 12 h are shown in Figs. 1c and 2c, respectively. There are no significant changes in these data over the room temper-

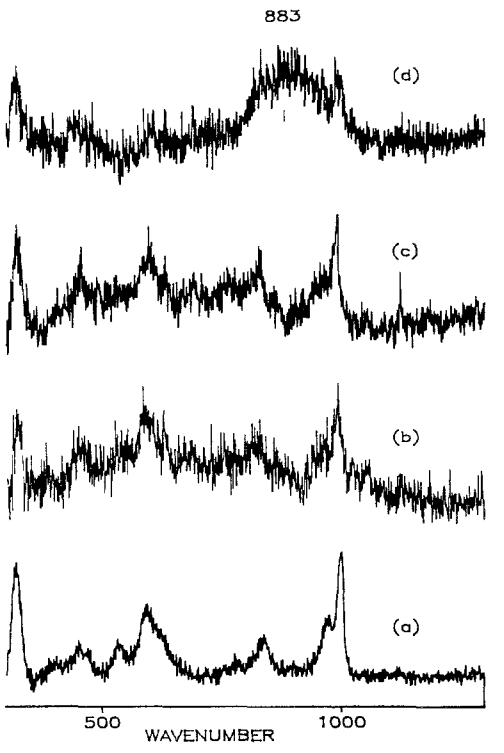

FIG. 2. Raman spectra of (a) $V_{10}O_{28}^{-6}$ ions in solution and (b) $V_{10}O_{28}$–$Mg_2Al(OH)_6$ at room temperature and heated to (c) 100°C and (d) 160°C (12 h at each temperature). Excitation, 457.9 nm.

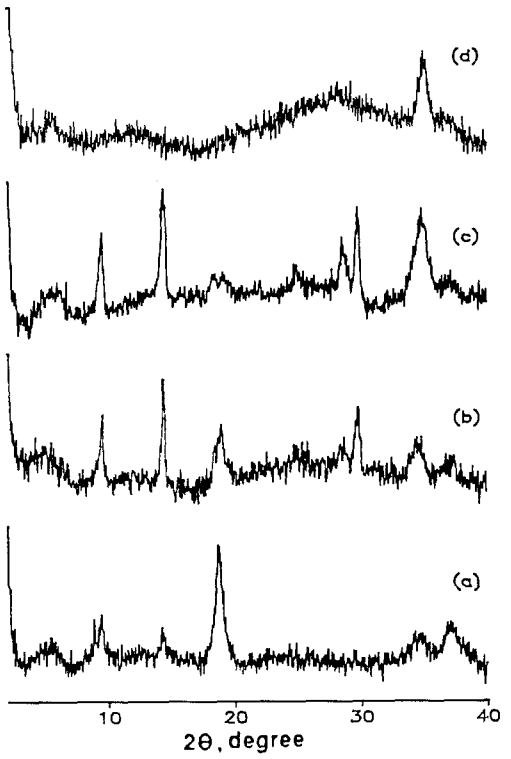

FIG. 3. Powder X-ray diffraction patterns of $V_{10}O_{28}$–$Mg_2Al(OH)_6$ heated to (a) 220°C, (b) 280°C, (c) 350°C, and (d) 450°C (12 h at each temperature).

ature spectra, indicating that the decavanadate ion as well as the framework remains intact. For a sample heated to 160°C, changes are apparent in the XRD and Raman spectrum (Figs. 1d and 2d). These include a new reflection at 4.76 Å and the appearance of a broad band centered at 880 cm^{-1}. The characteristic Raman bands of the decavanadate are still present, as are the XRD reflections characteristic of the decavanadate–hydrotalcite complex. However, it is clear that the decavanadate species is beginning to transform into other vanadate species at temperatures above 100°C. This becomes obvious upon examining the diffraction pattern and Raman spectrum of the sample heated to 220°C (Figs. 3a and 4a). Although the X-ray diffraction is still characteristic of a layered compound with three (001) reflections, the peaks characteristic of the decavanadate–hydrotalcite complex have all disappeared. The gallery height has decreased to 4.6 Å (d_{001} = 9.4 Å). There is only slight intensity in the Raman spectrum at ~1000 cm^{-1}, which is characteristic of the V–O stretch of the nonbonded oxygen atom of the $V_{10}O_{28}^{-6}$ ion. The prominent Raman bands occur at 870 cm^{-1}, with shoulders at 800 and 960 cm^{-1}. Monomeric and dimeric vanadate ions exhibit prominent Raman bands in the region 800–900 cm^{-1} (*29*). For example, the strongest bands in the spectra of VO_4^{-3}, HVO_4^{-2}, $V_2O_7^{-4}$, and $HV_2O_7^{-3}$ occur at 827, 877, 880, and 877 cm^{-1}, respectively. Cyclic metavanadate structures $(VO_3)_n^{n-}$ (where n = 3, 4) exhibit strong bands around 950 cm^{-1}. These bands are all assigned to symmetric stretching motions of the VO_3 and VO_2 groups. Clearly, the decavanadate ion is losing its integrity

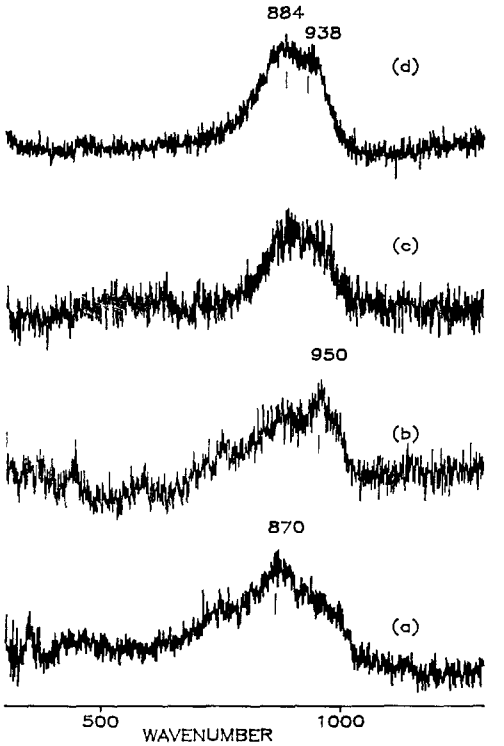

FIG. 4. Raman spectra of $V_{10}O_{28}$–$Mg_2Al(OH)_6$ heated to (a) 220°C, (b) 280°C, (c) 350°C, and (d) 450°C (12 h at each temperature). Excitation, 457.9 nm.

and transforming to simpler vanadate ions at temperatures beyond 160°C. Samples heated to 280°C still exhibit a layered structure (Fig. 3b), but prominent reflections are also present at $d = 3.0, 2.57$ Å. In the Raman spectrum, the peak at 950 cm^{-1} emerges as the strongest peak, with shoulders at 870 and 750 cm^{-1} (Fig. 4b). We propose that the interlayer chemistry occurring between 160–280°C can best be described as the depolymerization of the decavanadate ion:

$$V_{10}O_{28}^{-6} + 3H_2O \rightarrow 3V_3O_9^{-3} + HVO_4^{-2} + 5H^+. \quad (1)$$

The kinetics of this reaction has been reported to be slow at room temperature (*30*). However, as we discuss later, the high charge densities of the layer and the anion as well as elevated temperatures can promote this reaction. The Raman bands at 950 and 870 cm^{-1} observed at 280°C are characteristic of $V_3O_9^{-3}$ and HVO_4^{-2}, respectively (*29*). The considerable intensity in the region around 800 cm^{-1} could be due to VO_4^{-3} (827 cm^{-1}, νVO_2), formed by deprotonation of HVO_4^{-2}. The interlayer distance of ~4.6 Å corresponds well to the width of the $V_3O_9^{-3}$ ion (~5 Å). Upon heating to 350°C, the Raman spectrum sharpens up with no contribution below 800 cm^{-1} and the peak is observed at ~920 cm^{-1} (Fig. 4c). The diffraction pattern still shows the layer structure, along with the $d = 3.00$ and 2.57 Å reflections (Fig. 3c). The samples activated at 450°C show a Raman spectrum very similar to that of the 350°C sample, except that the two peaks at 884 and 938 cm^{-1} can now be clearly discerned (Fig. 4d). However, the diffraction pattern indicates that the layer structure is no longer intact and only a large angle reflection at 2.47 Å is observed (Fig. 3d). The vanadate species, at least as evidenced from the Raman spectrum, does not change between 350 and 450°C although the layer structure of the framework collapses in this temperature range. We assign the Raman bands at 884 and 938 cm^{-1} to a chainlike polymeric metavanadate species $(-O-VO_2-O-VO_2)_n$ on

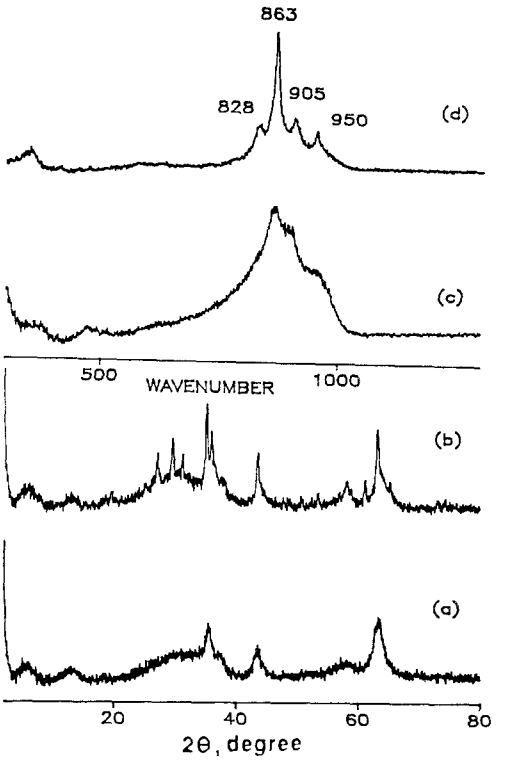

FIG. 5. Powder X-ray diffraction (a,b) and Raman spectra of $V_{10}O_{28}$–$Mg_2Al(OH)_6$ (c,d) heated to 550 and 650°C, respectively (12 h at each temperature).

the basis of reported studies of metavanadates in solution and in solid state (*31*). For example, KVO_3 in solution exhibits bands at 945 and 860 cm^{-1} and in solid state at 940 and 910 cm^{-1} (*2*). These vibrations arise from stretching motions of the VO_2 unit. The reaction of the vanadate species occurring between 220 and 450°C can best be described as

$$n(V_3O_9)^{-3} \rightarrow 3n(VO_3)^-. \quad (2)$$

Upon heating the decavanadate–hydrotalcite sample to 550°C, sharp Raman bands appear at 825, 860, 905, and 955 cm^{-1} on the broad metavanadate peak (Fig. 5c). With increase in temperature to 650°C, the metavanadate peak disappears altogether and only the sharp bands remain (Fig. 5d). The powder diffraction patterns of these samples are shown in Figs. 5a and 5b. The Raman

spectra are characteristic of α-$Mg_2V_2O_7$ (950, 905 cm^{-1}) and $Mg_3(VO_4)_2$ (863, 828 cm^{-1}) (*32*). The X-ray diffraction peaks at 550°C are characteristic of a spinel structure ($MgAl_2O_4$, 2.52, 2.02, and 1.43 Å) (*33*) whereas at 650°C, reflections are characteristic of $Mg_3(VO_4)_2$ (3.28, 3.02, 2.55, and 2.49 Å) (*34*). The reflections due to α-$Mg_2V_2O_7$ are not observed. As seen from the Raman spectrum, they form the minor component. Therefore, between the temperature ranges of 450–650°C, reaction between the vanadate species and the collapsed framework species are occurring. Previous studies of the thermal decomposition of the $Mg_2Al(OH)_6^+$ framework has shown that poorly crystalline MgO is formed at temperatures in excess of 500°C (*27*). In the presence of metavanadate, reactions schematically represented as

$$MgO + (VO_3)_n^{n-} \rightarrow Mg_2V_2O_7 + Mg_3(VO_4)_2 \quad (3)$$

can proceed readily. Only the α-form of $Mg_2V_2O_7$ is observed, since temperatures in excess of 700°C are required to form the β- and γ-forms (*30*).

Further characterization of this system was done by examining the vanadium XANES data for the thermally treated decavanadate–hydrotalcite samples and model systems. The X-ray absorption near-edge structure (XANES) within ~100 eV of the threshold absorption has been shown to have considerable structural information (*35–38*). Figures 6a–6d show the normalized V *K*-edge XANES spectra of the decavanadate–hydrotalcite samples heated to 100, 200, 350, and 450°C, respectively. The characteristic features of the V XANES spectrum include a pre-edge absorption (~0 eV) assigned to a $1s \rightarrow 3d$ transition. Vanadium pentoxide was used as the standard to define the origin of the pre-edge absorption peak. This dipole forbidden transition typically derives intensity by the mixing of the $3d$ orbitals with $4p$ metal and $2p$ ligand orbitals. This mixing is promoted by the lowering of symmetry around the vanadium atom from strictly octahedral to distorted octahedral and tetrahedral structures, respectively (*35*). It is clear from Fig. 6 that the intensity of this peak increases as the decavanadate–hydrotalcite sample is heated from 100 to 450°C and can be correlated with the change in V geometry from distorted octahedron ($V_{10}O_{28}^{-6}$) to tetrahedral structures ($(VO_3)_n^n$) upon thermal decomposition, in agreement with the Raman studies. The small change in the peak position (Δ = 0.6 eV) of this band upon thermal treatment is indicative of the retention of the +5 oxidation state during thermal treatment. The prominent band above the absorption edge is due to the $1s \rightarrow 4p$ transition and is part of the continuum, where features due to multiple scattering resonances that are sensitive to coordination geometry and inter-

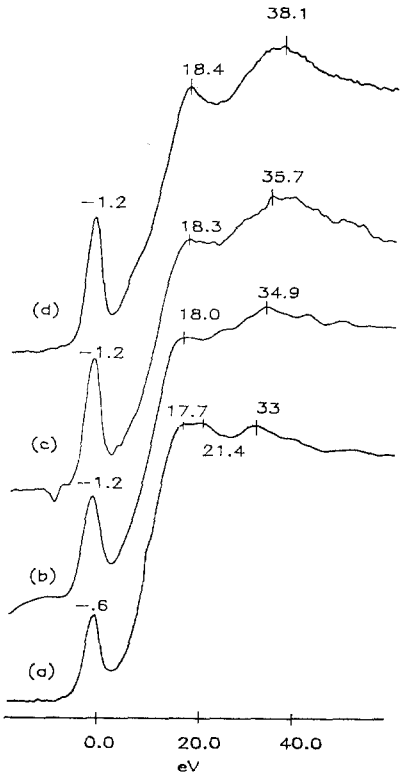

FIG. 6. Vanadium *K*-edge XANES spectra of $V_{10}O_{28}$–$Mg_2Al(OH)_6$ heated to (a) 100°C, (b) 220°C, (c) 350°C, and (d) 450°C.

atomic distances are also observed. We have compared the edge profile for the samples at 350 and 450°C treatment with a variety of model vanadium oxide systems that have been published and find the best correlations with tetrahedral vanadate, as in NH_4VO_3 and vanadinite ($Pb_5(VO_4)_3Cl$) (*35*). These results are consistent with the previously discussed Raman spectra of these systems.

DISCUSSION

From the thermal decomposition data (XRD, Raman, XANES) presented above, we can distinguish between three temperatures ranges. At temperatures below 350°C, the metal hydroxide framework remains more or less intact, but the intercalated decavanadate ion reacts with interlayer water molecules to form metavanadates. This is similar to our observations for the $LiAl_2(OH)_6$–V_2O_7 system, in which $V_2O_7^{-4}$ was found to polymerize to metavanadates (*17*). In both these instances, it is clear that even though the framework structure is remaining intact up to 350°C, interlayer chemistry involving the vanadate species is beginning at temperatures as low as 100°C. This is somewhat unique to the layered metal hydroxide supports. Previous studies on alumina supports prepared by impregnation of vanadate solutions have shown that both the tetrahedral $V_2O_7^{-6}$ and octahedral $V_{10}O_{28}^{-6}$ species maintain their structural integrity up to calcination temperatures of 450°C (*39, 40*). The question then arises as to what is the cause of the thermal instability of the decavanadate ion in the hydrotalcite. The driving force for the decavanadate decomposition in the hydrotalcite can be rationalized on the basis of the high charge density of the framework and the intercalated anion. There is some controversy in the literature about the exact value of the charge density for $Mg_2Al(OH)_6^+$-type compounds (*12, 21, 23*). Values of 16.6 and 25 $Å^2$ per unit positive charge on the layer have been reported. For an ordered arrangement of cations in a hexagonal cell, we calculate a value of 25 $Å^2$ per charge (*13*). For the decavanadate anion, we estimate from the crystallographic data that a unit negative charge is distributed over an area of 15 $Å^2$ (*41*). Thus, in the case of the decavanadate-pillared hydrotalcite, the charge density in the interlayers is more localized than the metal hydroxide layer. The presence of high dielectric constant water molecules helps stabilize the electrostatic interactions. Thermal gravimetric analysis of hydrotalcites has shown that water loss from the interlayers begins at 100°C and continues up to 300°C (*10, 27*). We propose that this water loss brings about the chemical changes associated with the decavanadate ion. With increasing water loss from the interlayers, the decavanadate ion due to its high charge density promotes the polarization and hydrolysis of the remaining water molecules, resulting in formation of OH^- and H^+ ions. The hydroxide ions are responsible for the decomposition of the decavanadate ion into lower charge density cyclic metavanadate species.

At temperatures between 350 and 450°C, the layer structure collapses but without any significant chemical reaction between the vanadate and the framework species. Thermal analysis studies of a series of hydrotalcites with varying metal ion compositions have shown that dehydroxylation begins at temperatures greater than 350°C (*27, 28, 42*). In some cases, the layer structure can also be restored by rehydration, even after treatment at temperatures as high as 450°C (*27*).

It has been recognized that at temperatures of 500°C and beyond, the framework atoms begin to form metal oxides (*27*). In this study, we find that magnesium oxide then reacts with the metavanadate species to form specific magnesium vanadates, namely, α-$Mg_2V_2O_7$ and $Mg_3(VO_4)_2$.

The most important conclusion of this study is that the interlayer space in the hydrotalcite provides a reactive environment for the polyoxometalates, even upon gentle thermal treatment. Therefore, in the preparation of pillared catalytic materials by use

of this approach, consideration must be given to the fact that the polyoxometalate ion may lose its structural integrity, even though the layered structure may remain intact. This study has also shown that Raman spectroscopy and XANES can provide structural information about the various intercalated and product species.

ACKNOWLEDGMENTS

We thank NSF (CHE-8510614) for partial support of this work. The XANES experiments were done at the National Synchroton Light Source, Brookhaven National Laboratory (DOE Contract DE-AC02-76CH00016). We thank Mr. Chris Bowers, Mr. Dan Robbins, Dr. Geoffrey Woolery, and Professor James Alben for their help with the XANES experiments.

REFERENCES

1. Setton, R., *Synth. Met.* **23,** 467 (1988).
2. Lagaly, G., *Adv. Colloid Interface Sci.* **11,** 105 (1979).
3. Rudolf, P. R., and Clearfield, *Inorg. Chem.* **28,** 1706 (1989).
4. Pinnavaia, T. J., *Science* **220,** 365 (1983).
5. Reichle, W. T., *Chem. Tech.,* 58 (1986).
6. Inagaki, M., *J. Mater. Res.* **4,** 1560 (1989).
7. Occelli, M.L., *Ind. Eng. Chem. Prod. Res. Dev.* **22,** 553 (1983).
8. Lal, M., and Howe, A. T., *J. Solid State Chem.* **39,** 337 (1981).
9. Allmann, R., *Acta Crystallogr. B* **24,** 972 (1968).
10. Miyata, S., and Okada, A., *Clays Clay Miner.* **25,** 14 (1977).
11. Itaya, K., Chang, H., and Uchida, I., *Inorg. Chem.* **26,** 624 (1987).
12. Boehm, H., Steinle, J., and Vieweger, C., *Angew. Chem. Int. Ed. Engl.* **16,** 265 (1977).
13. Serna, C. J., Rendon, J. L., and Iglesias, J. E., *Clays Clay Miner.* **30,** 180 (1982).
14. Martin, K. J., and Pinnavaia, T. J., *J. Amer. Chem. Soc.* **108,** 541 (1986).
15. Schutz, A., and Biloen, P., *J. Solid State Chem.* **68,** 360 (1987).
16. Dutta, P. K., and Puri, M., *J. Phys. Chem* **93,** 376 (1989).
17. Dutta, P. K., and Twu, J., *J. Phys Chem.* **93,** 7863 (1989).
18. Plee, D., Gatineau, L., and Fripiat, J. J., *Clays Clay Miner.* **35,** 81 (1987).
19. Mortland, M. M., and Berkshier, V., *Clays Clay Miner.* **24,** 60 (1976).
20. Jones, W., *Catal. Today* **2,** 357 (1988).
21. Kwon, T., Tsigdinos, G. A., and Pinnavaia, T. J., *J. Amer. Chem. Soc.* **110,** 3653 (1988).
22. Drezdzon, M. A., *Inorg. Chem.* **27,** 4628 (1988).
23. Kwon T., and Pinnavaia, T. J., *Chem. Mater.* **1,** 381 (1989).
24. Woltermann, G. M., US Patent 4,454,244 (Expanded Layered Minerals, assigned to Ashland Oil) (1984).
25. Nakatsuka, T., Kawasaki, H., Yamashita, S., and Kohjiya, S., *Bull. Chem. Soc. Japan* **52,** 2449 (1979).
26. Kelkar, C. P., Schultz, A., and Marcelin, G., *ACS Symp. Ser.* **368,** 324 (1988).
27. Reichle, W. T., *J. Catal.* **94,** 547 (1985); Reichle, W. T., Kang, S. Y., and Everhardt, D. S., *J. Catal.* **101,** 352 (1986).
28. Busetto, G., DelPiero, G., Manara, G., Trifiro, F., and Vaccari, A., *J. Catal.* **85,** 260 (1984).
29. Griffith, W. P., and Wickins, T. D., *J. Chem. Soc. A,* 1087 (1966); Griffith, W. P., *J. Chem. Soc. A,* 905 (1967).
30. Baes, C. F., and Mesmer, R. E., "The Hydrolysis of Cations," p. 205. Wiley–Interscience, New York, 1976.
31. Onodera, S., and Ikegami, Y., *Inorg. Chem.* **19,** 615 (1980).
32. Hanuza, J., Trzebiatowska, B., and Oganowski, W., *J. Mol. Catal.* **29,** 109 (1985).
33. National Bureau of Standards Mono. 25, Sec. 9 (1971).
34. Clark, G. M., and Morley, R., *J. Solid State Chem.* **16,** 429 (1976).
35. Wong, J., Lytle, F. W., Messmer, R. P., and Maylotte, D. H., *Phys. Rev. B* **30,** 5596 (1984).
36. Bianconi, A., Fritsch, E., Calas, E., and Petiau, J., *Phys. Rev. B* **32,** 4292 (1985).
37. Tonaka, T., Nishimura, Y., Kawasaki, S., Funabiki, T., and Yoshida, S., *J. Chem. Soc. Chem. Comm.,* 506 (1987).
38. Woolery, G. L., Chin, A. A., Kirker, G. W., and Huss, A., Jr., *ACS Symp. Ser.* **375,** 215 (1988).
39. Coustumer, L. R., Taouk, B., LeMeur, M., Payen, E., Guelton, M., and Grimblot, J., *J. Phys. Chem.* **92,** 1230 (1988).
40. Roozeboom, F., Medema, J., and Gellings, P. J. G., *Z. Phys. Chem.* **111,** 215 (1978).
41. Evans, H. T., Jr., *Inorg. Chem.* **5,** 967 (1966).
42. Lal, M., and Howe, A. T., *J. Solid State Chem.* **39,** 368 (1981).